Applied Thermal Engineering 236 (2024) 121462

Contents lists available at ScienceDirect

Applied Thermal Engineering

journal homepage: www.elsevier.com/locate/apthermeng

Research Paper

Flow and thermal mixing characteristics of a multi-jet bypass flue with main flue baffles

Yize Zhang, Ao Zhang, Lei Zhang, Kelang Jin, Hao Zhou *

State Key Laboratory of Clean Energy Utilization, Institute for Thermal Power Engineering, Zhejiang University, Hangzhou 310027, China

ARTICLE INFO

Keywords:
Bypass flue
Baffle
Multiple jets
Mixing performance
Low load
Flow characteristics

ABSTRACT

The decrease of inlet flue temperature of denitrification reaction unit is a major challenge that restricts the low load operation of thermal power units. In this study, a new bypass flue heating technology based on multi-pipe and multipoint was proposed. The effect of different baffle openings (R_A), directions and position distance (D_b) on the mixing characteristics of multiple jets was quantitatively investigated by the experimental system. Combined with the simulation, the changes of the baffle on the multi-jet flow and mixing are revealed. The results show that the mixing temperature increases with increasing R_A, but high R_A leads to a significant increase in the thermal mixing temperature inhomogeneity (ζ_T). As R_A increases from 0.4 to 0.7, ζ_T rises from the minimum 0.368 to the maximum 0.559. The mixing temperature and ζ_T of the baffle in the +x direction are higher than those in the −x direction. When D_b increases from 70 mm to 130 mm, the maximum heating effect decreases from 25.97 °C to 18.89 °C, and ζ_T decreases gradually at $y/D_h = 1.25$. The findings provide guidance for bypass flue modification and low load denitrification in engineering.

1. Introduction

With the development of new energy, the thermal power flexibility transformation in China requires units to operate smoothly and reliably under low loads (less than 50 % of the rated power) [1]. A decrease in the inlet flue gas temperature of selective catalytic reduction (SCR) denitrification units is a major problem at low loads, resulting in the generation of ammonium bisulphate (ABS) [2]. ABS has a strong moisture absorption capacity and stickiness, and can adsorb fly ash deposited on the surface of the ammonia spray grid and catalyst, reducing the efficiency of the denitrification system [3]. It also leads to clogging and corrosion of the air preheater, causing unplanned boiler shutdowns and reducing the economic benefits of the power plant [4].

The flue gas bypass technology is widely used by power plants to solve the above problems caused by low load [5]. A bypass flue is opened at the outlet of a high-temperature reheater to extract high-temperature flue gas (HTFG). The HTFG with a temperature of approximately 400–500 °C is injected into the tail flue and mixed with the low-temperature flue gas (LTFG) to increase the inlet flue gas temperature of the SCR denitrification unit [6]. The thermal mixing of the bypass flue gases is based on the jets in the crossflow. This physical phenomenon is used in engineering practices in a wide range of fields, including aerospace fuel premixing [7], combustion instability control [8], component cooling [9], pollutant removal in thermal power generation [10], and nuclear reactor cooling [11]. Researchers have conducted extensive experimental and numerical simulations [12] for this study. A comprehensive study of a novel injection of multi-hydrogen jets in a cavity type flame holder under supersonic free-flow conditions has been carried out by Edalatpour et al. [13]. Moradi et al. investigated the effect of different shaped cavities as flame holder on the internal mixing efficiency of scramjet [14]. The relationship between the acoustic pressure and the exothermic rate of a nonstationary flame under an oxygen-containing jet crossflow was revealed by Tao et al. [15]. A correlation analysis of an oxygen-fuel crossflow jet on a thermoacoustic unsteady flame was performed in a model gas turbine chamber. Zhou et al. [16] combined micro-thermocouples and optical measurement techniques to study the flow and thermal fatigue phenomena near the weld seam in a thermally mixed tube flow downstream of a 90° T-junction. Lin et al. [17,18] combined experiments and computational fluid dynamics (CFD) numerical simulations to investigate the thermal mixing and counterflow characteristics of cold-water branches and hot-water mains in T-junctions. The research on the application of single jet in engineering has been quite sufficient. The single-pipe bypass technology based on the principle of single jet has drawbacks. This method causes large deviations in temperature and concentration after hot

* Corresponding author at: State Key Laboratory of Clean Energy Utilization, Zhejiang University, Zheda Road 38, Hangzhou 310027, China.
E-mail address: zhouhao@zju.edu.cn (H. Zhou).

https://doi.org/10.1016/j.applthermaleng.2023.121462
Received 31 May 2023; Received in revised form 12 August 2023; Accepted 29 August 2023
Available online 30 August 2023

Nomenclature

D_h	hydraulic diameter, mm
W	wetted perimeter, mm
A_m	cross-sectional area of the main flue, m^2
A_J	cross-sectional area of jet inlet, m^2
U_J	jet velocity, m/s
Um	mainstream velocity, m/s
ρ_J	jet gas density, kg/m^3
ρ_m	mainstream gas density, kg/m^3
R_u	velocity ratio, $R_u = U_J / U_m$, dimensionless
R_m	flow ratio, $R_m = \rho_J A_J U_J / \rho_m A_m U_m$, dimensionless
D_b	distance between the baffle and the center of the jet pipe, mm
R_A	ratio of baffle area in the main flue, $R_A = A_b / A_m$, dimensionless
R_ρ	density ratio, $R_\rho = \rho_J / \rho_m$, dimensionless
d	jet hole diameter, mm
ΔT	temperature difference, °C
ζ_T	inhomogeneity parameter of temperature distribution
T	time-averaged temperature of each measurement point, °C
$\overline{T}$	surface average temperature, °C
T_0	mainstream temperature, °C
T_{max}	maximum temperature within the y/Dh = 1.25 cross-section, °C
σ_T	standard deviation of the measured temperatures on the surface
θ	dimensionless temperature in the measurement plane

Abbreviations

SCR	selective catalytic reduction
ABS	ammonium bisulfate
HTFG	high-temperature flue gas
LTFG	low-temperature flue gas
HLTFG	high- and low-temperature flue gases
CFD	computational fluid dynamics

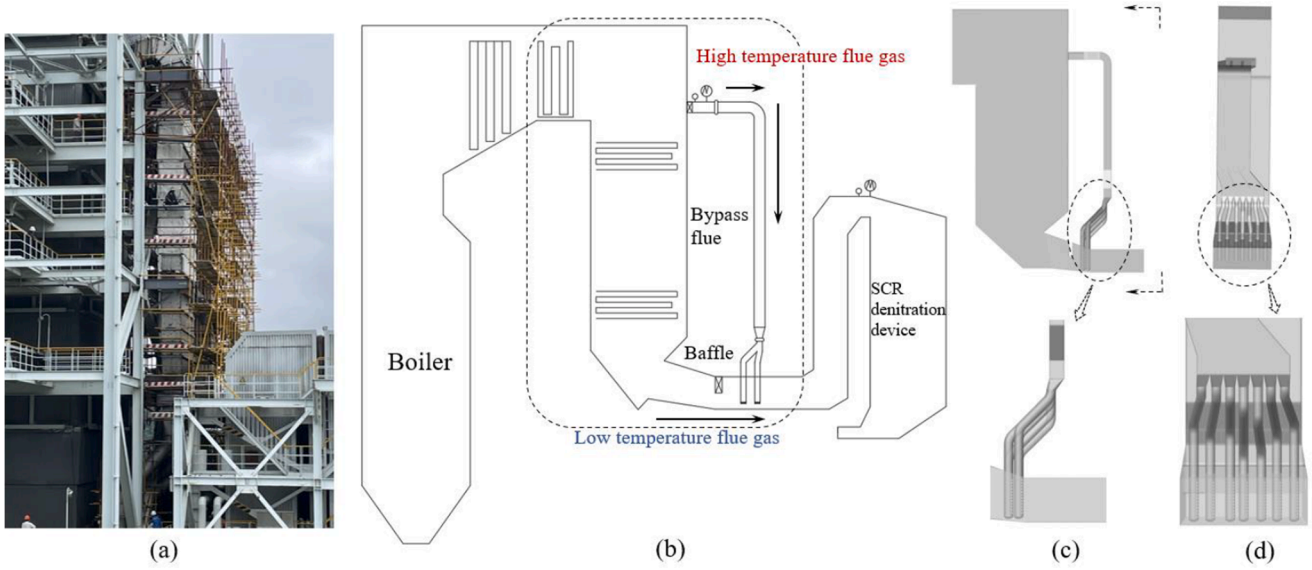

Fig. 1. The multi-pipe bypass flue preheating technology. (a) Physical photo; (b) Schematic diagram; (c) and (d) Model.

mixing of high and low temperature flue gas (HLTFG), resulting in low load denitrification efficiency unable to meet the requirements. Therefore, we proposed a new flue gas bypass heating technology based on multi-tube and multi-point mixing, as shown in Fig. 1(a). At present, the multi-jet HLTFG flow and hot mixing characteristics of this technology are rarely studied. Similarly, this technology is limited by the onsite structural situation, resulting in several bends in the distribution of multiple branches. This results in a low volume of flue gas being extracted from the bypass flue with high resistance. By installing insert valves in the main flue and controlling the opening of the baffle doors, the resistance of the main flue is adjusted to increase the flow of the HTFG in the bypass flue and change the flow rate in the main and bypass flues.

Baffles are common and effective tools in practical engineering applications and play an important role in improving the structure of the flow field and enhancing the heat exchange effect [19]. Wu et al. [20] used CFD and virtual reality to optimize the chamber design using multiple baffles to reduce the formation of debris at the top of the urea decomposition chamber in a power plant. Boruah et al. [21] numerically analyzed the thermohydraulic and entropy production characteristics of hybrid convection in a backward-stepped duct with baffles. Chen et al. [22] studied the effects of baffle types on the heat transfer and fluid flow characteristics of shell-and tube-heat exchangers by a hot and cold-water heat exchange system. Our previous study explored thermal mixing methods applicable to low loads in bypass flue gas technology and the effect of temperature differences and flow rates of HLTFG on thermal mixing characteristics through experiments and CFD [23]. However, the multi-point thermal mixing method with baffles in the main flue has not yet been investigated. The parameters of the baffle will inevitably affect the flow and thermal mixing characteristics. Therefore, we are motivated to fill the gap in the research of this technology by exploring the effect of baffles on the flow and mixing of multi-jet streams.

Considering the repetitive nature of the lower branch structure of a bypass flue, this study focused on a single-branch pipe. Detailed experiments and numerical simulations were performed to investigate this phenomenon. In this study, adjustable baffles were added to a constructed experimental system for the turbulent thermal mixing of

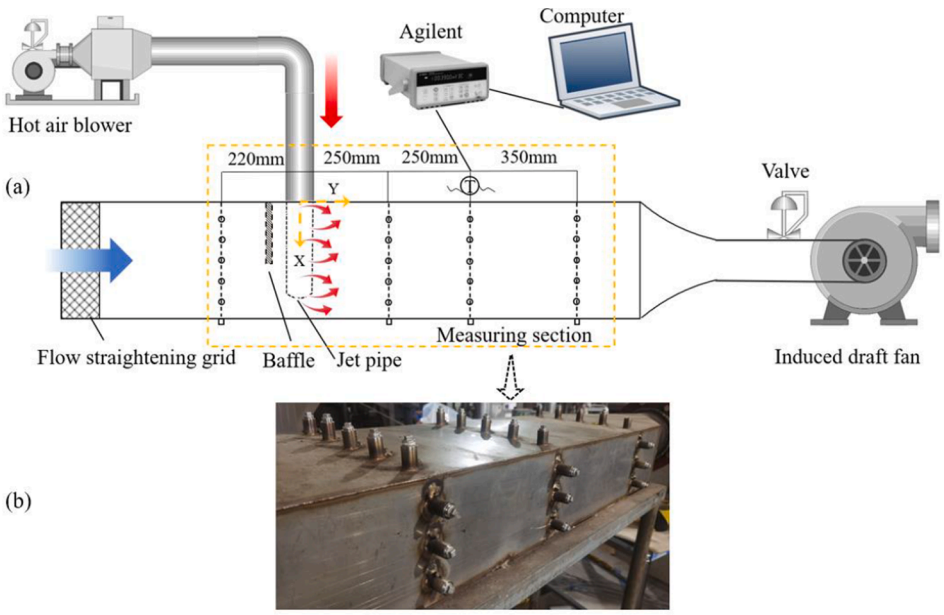

Fig. 2. Experimental system: (a) schematic diagram of the apparatus and (b) physical view of the measurement area.

different gases to simulate the adjustment of thermal mixing effect through the baffle valve. The effects of the baffle installation direction, baffle position and baffle door opening on the HLTFG flow and thermal mixing characteristics were investigated. Combined with contour plots, the direct change of baffles on multi-jet flow and thermal mixing is revealed. Through detailed parametric investigation, the relationship of each factor with the warming effect and temperature distribution inhomogeneity coefficient after thermal mixing of multi-jet high and low temperature gases is obtained, respectively. The study results provide an important reference for thermal power flexibility retrofitting and are equally significant for ensuring the stable low-load operation of SCR denitrification systems in thermal power units during peaking.

2. Experimental setup

2.1. Experimental systems

A schematic diagram of the experimental setup is shown in Fig. 2(a). The system comprises a gas generation unit, measurement area, and data acquisition unit. The experimental procedure used air instead of flue gas in the simulation studies. The gas generation unit consists of a hot air blower and an induced draft fan. The outlet of the hot blower was connected to a jet pipe to maintain the temperature and velocity of the high-temperature jet gas. The induced draft fan was connected to the main flow duct in the measurement zone to maintain the cold flow gas velocity in the duct. A flow-straightening grid was installed at the main flue inlet to distribute the airflow evenly. Thermal mixing of HLTFG occurred in the main flow flue. The experimental model was scaled and simulated at a 1:10 ratio according to the engineering reality. The measurement zone had a cross section of 300 mm × 150 mm and a hydraulic diameter of D_h = 200 mm. The equation for D_h is as follows:

$$D_h = 4\frac{A_m}{W} = 4 \times \frac{150 \times 300}{2(150+300)} = 200mm \quad (1)$$

where A_m denotes the cross-sectional area of the measurement area, and W represents the wet perimeter.

A measuring zone was established with four measuring surfaces along the gas flow direction. Three measuring holes were set on the side of each measurement surface, and five measuring holes were set above. The origin of the spatial coordinates of the experimental model was positioned at the intersection of the central axis of the multi-hole jet pipe and the side of the mainstream flue, as shown in Figs. 2(a) and 4(a). The four measuring planes were located at Y = −220 mm, 250, 500 and 850 mm. The first measurement plane was located before the thermal mixing zone and was used to verify the relative uniformity of the velocity distribution of the gas as it entered the main flue.

The physical and structural multihole jet pipes installed in the experimental system are shown in Fig. 3. A previous study showed that the pipe had excellent thermal mixing characteristics, and the open hole at the base of the jet pipe effectively prevented the jet hole from being blocked by ash accumulation [24].

2.2. Experiment case

The bypass flue extracts the HTFG from the final superheater outlet for heating the LTFG flowing through the economizer outlet. According to the actual measured data of a power plant boiler, when operating at low load (30 % boiler rated power), the temperature difference between the above two locations is 180–270 °C. The flue gas flow velocity in the tail flue between the economizer outlet and the SCR inlet was approximately 8–12 m/s. Therefore, the temperature difference between HTFG and LTFG in the experimental conditions is maintained at 200 °C. The LTFG flow velocity in the main flue was set to 10 m/s, and the HTFG inlet velocity was 18 m/s, as listed in Table 1, where R_u represents the velocity ratio of the jet and the main flow, and R_m indicates the flow ratio of the jet and the main flow.

To regulate the resistance in the main flue, the baffle doors installed in power stations are mostly of the installation valve type. Based on practical applications, experiments were conducted to investigate the effects of the baffle installation direction and, baffle position and opening on the HLTFG flow and thermal mixing characteristics, as detailed in Table 2. The baffle installation direction includes the x-axis positive and negative directions. The baffle position is determined by the distance (D_b) between the baffle and center of the jet pipe. The baffle area ratio (R_A) quantifies the baffle opening within the main flue cross-section. The equation for R_A is as follows:

$$R_A = \frac{A_b}{A_m} \quad (2)$$

where A_b and A_m denote the baffle area and main flue cross-section area, respectively.

The specific physical models and factor variations are shown in

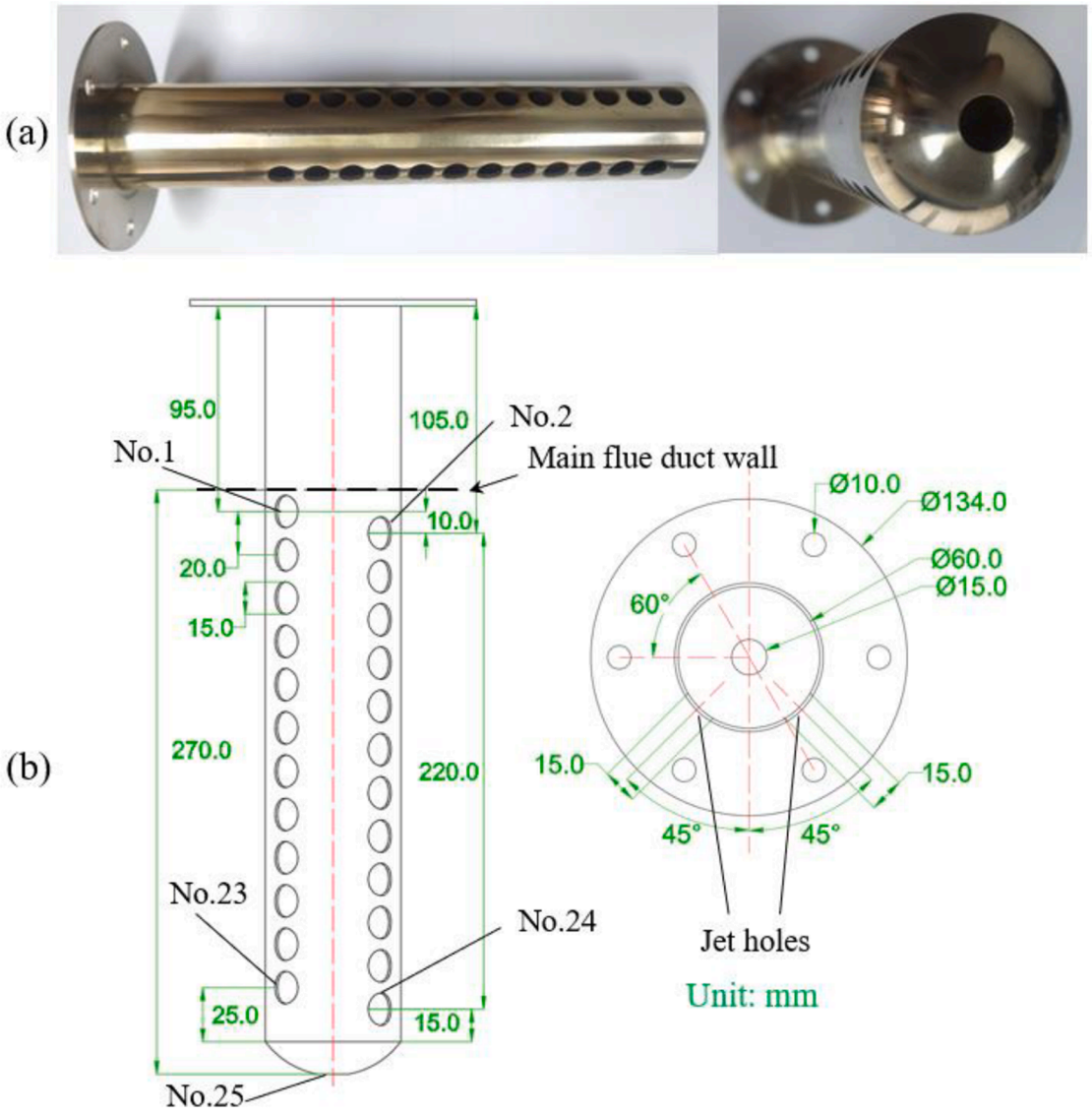

Fig. 3. Physical structure of the multi-hole jet pipe.

Table 1
Experimental conditions.

	Temperature (°C)	Velocity (m/s)	$R_u = \frac{U_J}{U_m}$	$R_m = \frac{\rho_J A_J U_J}{\rho_m A_m U_m}(\%)$
Jet flow	220	$U_J = 18$	1.8	11.31 %
Main flow	20	$U_m = 10$		

Fig. 4. Case 1 was the original case in which no baffle was installed in the main flue. In practice, at small baffle door openings ($R_A < 0.2$), the resistance of the main flue increases slightly, and the bypass pumping capacity increases slightly. When the baffle door opening is high (above 0.7), the resistance is too high in practice, and the local flow rate is too fast, posing certain safety risks. Therefore, the experimental baffle area ratio in the main flue was set between 0.2 and 0.7.

2.3. Scalar field measurement

A hot-wire anemometer (KAMOMAX MODEL) was used to measure the flow distribution of the multihole pipe jet orifice with an accuracy of ±3.0 % and a measurement resolution of 0.01 m/s. K-type thermocouples connected to an Agilent 34970A instrument were used to measure the time-averaged temperature. The temperature range of K-type thermocouples is 0–1100 °C with a measurement accuracy of

Table 2
Experimental cases.

Case	Baffle direction	D_b (mm)	Dimensionless distance	R_A
1	No baffle	–	–	–
2	+x	70	0.35	0.2
3	+x	70	0.35	0.3
4	+x	70	0.35	0.4
5	+x	70	0.35	0.5
6	+x	70	0.35	0.6
7	+x	70	0.35	0.7
8	−x	70	0.35	0.3
9	−x	70	0.35	0.5
10	−x	70	0.35	0.7
11	+x	100	0.50	0.3
12	+x	100	0.50	0.5
13	+x	100	0.50	0.7
14	+x	130	0.65	0.3
15	+x	130	0.65	0.5
16	+x	130	0.65	0.7

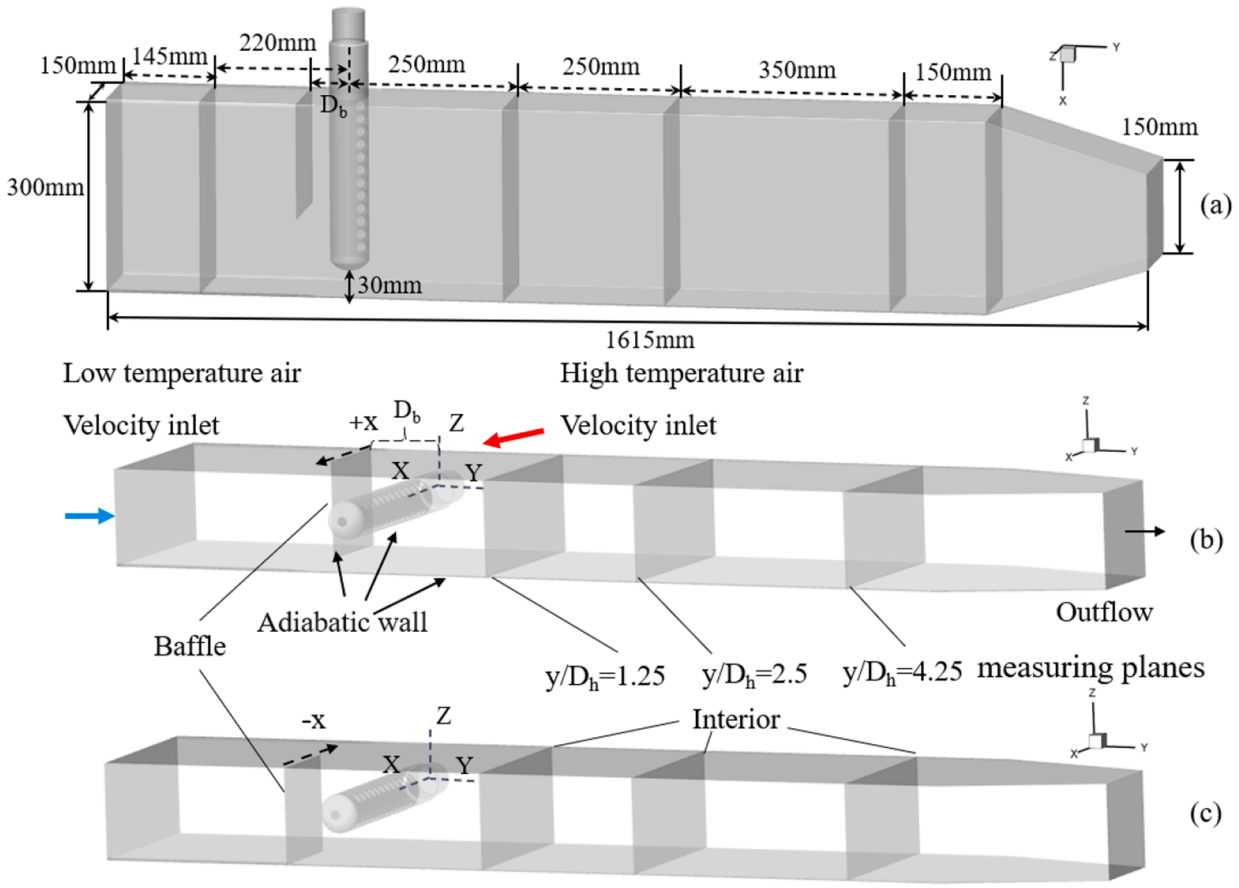

Fig. 4. Simulation geometry and boundary conditions: (a) model size, (b) baffle +x direction, (c) −x direction.

±0.75 %. The thermocouple used is 1 mm in diameter. The thermocouple used is 1 mm in diameter. The thermocouple is uniformly fixed on a 2 mm diameter metal rod and assembled into a temperature measuring gun. The temperature field of the cross-section was measured by extending the gun into the measurement hole. Eighteen thermocouples were used to obtain the temperature distribution along the horizontal direction of the primary flow pipe. Similarly, 15 thermocouples were used in the vertical direction. The thermocouple is connected to the data collector (Agilent 34970A) for temperature signal acquisition. The average temperature was measured over a 120 s period to ensure accuracy. The Agilent data sampling frequency was set at 2 Hz.

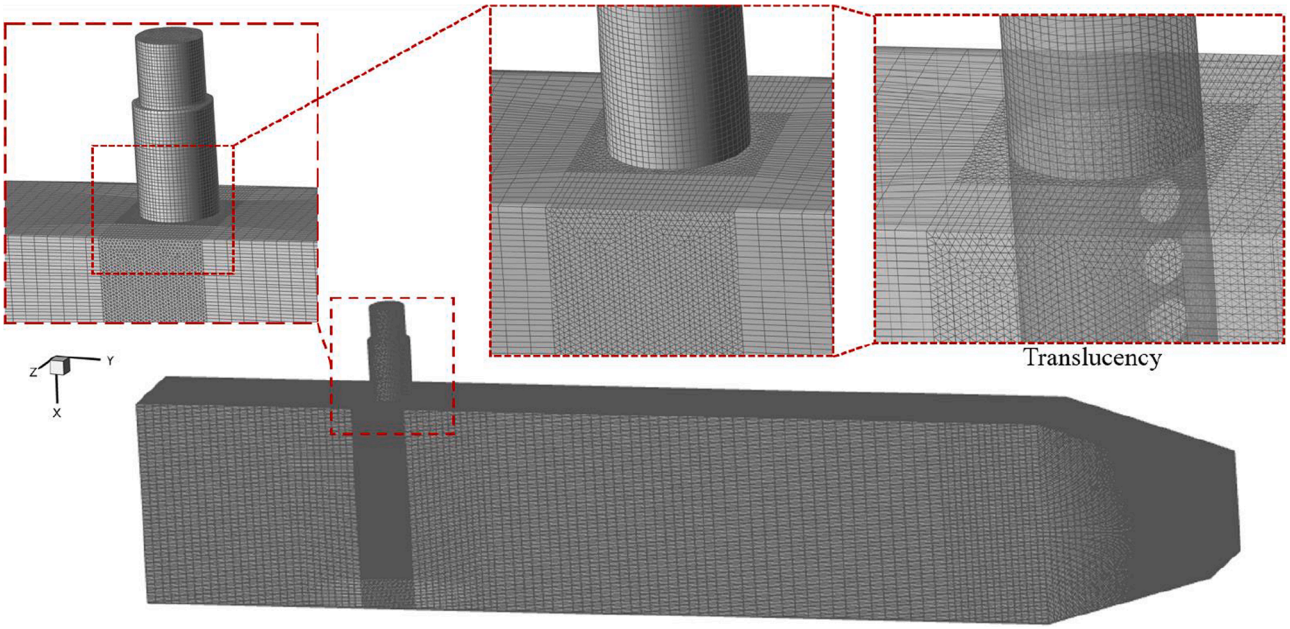

Fig. 5. The grid structure used for the simulations in this study.

Table 3
Grid independence test and verification results (Case 1).

Grid	$\overline{T}_{1.25}$(°C)	Error (%)	$\overline{T}_{2.5}$(°C)	Error (%)	$\overline{T}_{4.25}$(°C)	Error (%)	y + Max.
861,476	31.725	–	29.928	–	29.234	–	111.40
1,271,069	31.356	1.16 %	29.941	0.04 %	29.245	0.04 %	131.30
1,700,518	31.111	0.78 %	29.804	0.46 %	29.137	0.37 %	152.68
2,154,111	31.617	1.63 %	29.920	0.39 %	29.210	0.25 %	112.75
4,921,617	30.814	2.54 %	29.247	2.25 %	28.719	1.68 %	150.33

In total, 129 sampling points within each measurement plane were used for data processing.

3. Simulation

To further investigate the local flow and thermal mixing characteristics, model building and meshing were performed using by Gambit software, and numerical simulations were performed by using ANSYS-FLUENT. The flows were treated as steady-state flows of incompressible fluids. The influence of radiative heat transfer was ignored. A pressure-based solver is used to solve the nonlinear governing equations. The governing equations are as follows:

The continuity equation:

$$\frac{\partial(\rho u_i)}{\partial x_i} = 0 \tag{3}$$

The momentum equation:

$$\frac{\partial(\rho u_i u_j)}{\partial x_i} = -\frac{\partial P}{\partial x_i} + \frac{\partial}{\partial x_i}\left[(\mu + \mu_t)\left(\frac{\partial u_j}{\partial x_i} + \frac{\partial u_i}{\partial x_j}\right)\right] \tag{4}$$

The energy equation:

$$\frac{\partial(\rho u_i T)}{\partial x_i} = \frac{\partial}{\partial x_i}\left[\left(\frac{\mu}{P_r} + \frac{\mu_t}{P_{r_t}}\right)\frac{\partial T}{\partial x_i}\right] \tag{5}$$

The physical model is modeled according to the measured part of the experimental system. The size of the model is shown in Fig. 4(a), with a total length of 1615 mm. The outlet is connected with the flue pipe of the induced draft fan. So, the section is reduced. The positions of the jet pipe, baffle and measuring surfaces are exactly the same as those of the experiment. The bottom of the jet pipe is 30 mm away from the tube wall. The structure size of the jet pipe is shown in Fig. 3. The computational cases are the same as the experimental situations. The boundary conditions are shown in Fig. 4. The high-temperature jet and low-temperature main flow inlets are set to the "velocity inlet" condition, and the computational domain outlet is set to the "outflow" condition. Other wall surfaces including baffles and pipe walls are set as no-slip adiabatic walls.

The Realizable k-ε model with standard wall functions was used as the turbulence model in the simulations. The model was able to accurately predict the spreading of circular hole jets.[25,26] The standard wall function was used for boundary layer problems, and can be accurately solved for wall boundary flows with extremely high Reynolds numbers [27]. The SIMPLE algorithm was used to solve the finite difference equations for the coupling of velocity and pressure. The mass, momentum and energy equations were discretized using the second-order upwind scheme. The first-order upwind scheme was used for turbulent kinetic energy and turbulent dissipation rate. The residuals of all governing equations during the iteration are less than 10^{-5}, which is considered as the criterion for computational convergence.

The grid structure used for the simulations in this study is shown in Fig. 5. Structural meshing was performed in relatively regular areas, and unstructured meshing was performed on parts of the jet pipe. The grid was refined for the area where the baffle and jet pipe are placed. The average size of the mesh in the structured area is 10 mm. The size of the refined mesh is 2 mm, which is much smaller than the rest of the structured area. The average size of the mesh in the structured area is 10 mm. The transition area is segmented to achieve smooth mesh division and ensure mesh quality. The maximum Aspect Ratio of the mesh is 9.8, and most of the meshes are less than 5, which proves that the mesh

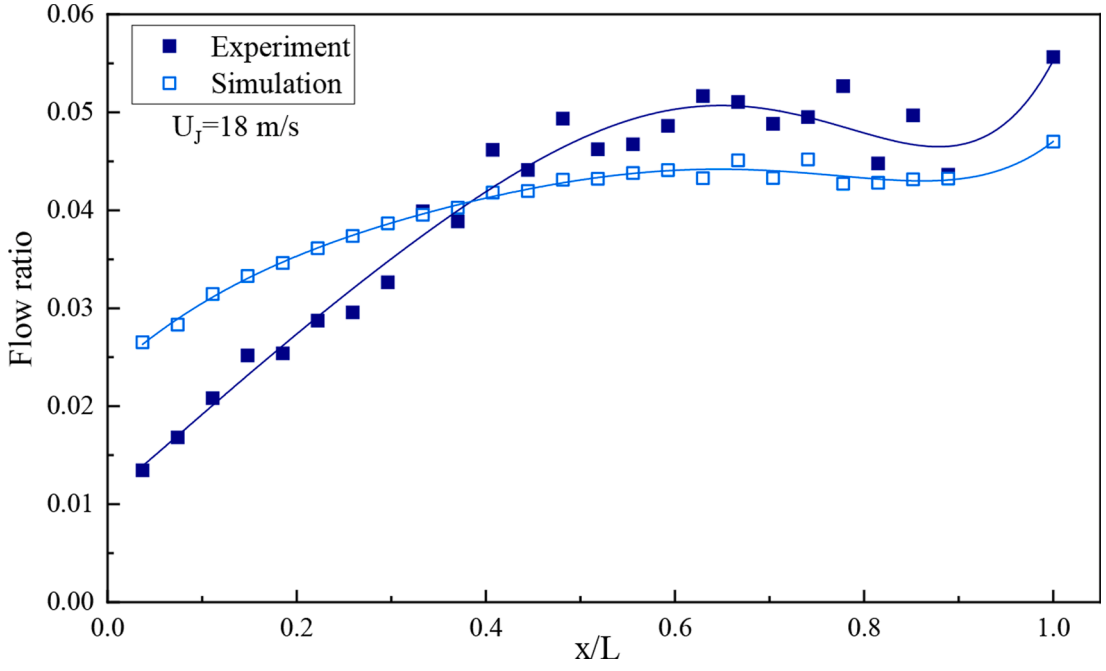

Fig. 6. Distribution of jet flow along a multi-hole jet pipe. (The ordinate axis is the ratio of jet hole flow to total flow in the pipe).

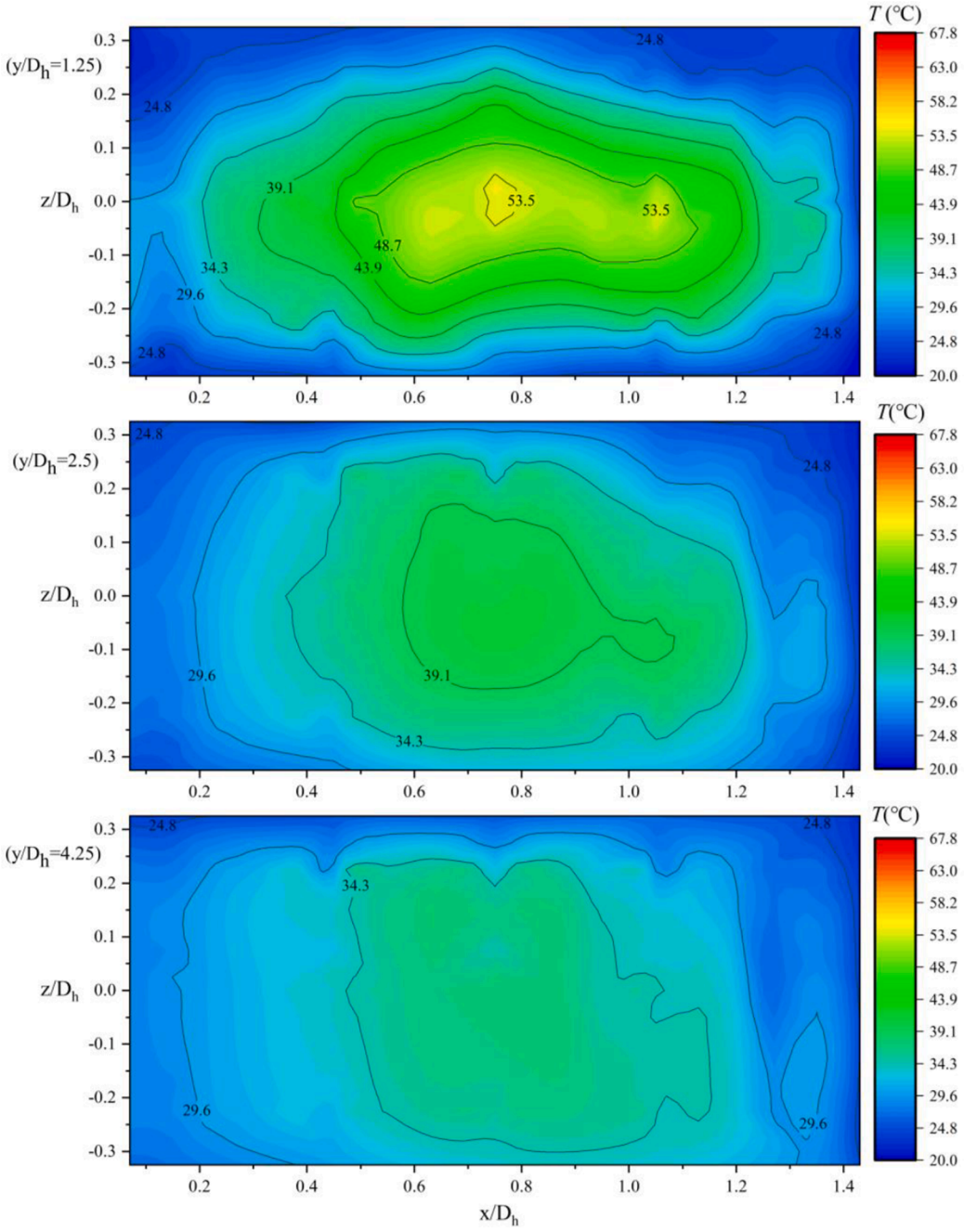

Fig. 7. Temperature distribution for case 1 (No baffle) at y/Dh = 1.25, y/Dh = 2.5 and y/Dh = 4.25.

quality is excellent. The y+ values were counted in the grid-independence validation and are shown in Table 3. The results are consistent with the range of applicability of the high Reynolds number turbulence model.

The initial model (Case 1) was selected as the grid independence verification object. Three cross sections $y/D_h = 1.25$, 2.5 and 4.25 were used as detection planes to verify the mesh independence results. By increasing the number of nodes, the total mesh is uniformly increased. According to Eq. (6), the result error is calculated, and the statistical results are shown in Table 3.

$$error = \frac{|x_n - x_{n+1}|}{x_n} \times 100\% \tag{6}$$

where x_n indicates the calculation result, and n indicates the n-th calculated case. As shown in Table 2, when the number of grids increases from 861,476 to 1,700,518, the surface-averaged temperature error of $y/D_h = 1.25$ decreases. The error value is less than 1 %. When the number of grids increases from 1,700,518 to 4,921,617, the face-averaged temperature error increases significantly and the computational stability deteriorates. When the grid is less than 2,154,111, the average surface temperature errors of the other two sections are less than 1 %, which meets the requirement of calculation accuracy. In summary, the number of simulation grids used is 1,271,069, which ensures the accuracy and saves the calculation time.

4. Results and discussion

Using $U_J = 18$ m/s as the initial velocity of the jet inlet, experimental measurements and simulations were performed on the flow distribution of the multi-hole jet pipe. The statistical results are shown in Fig. 6. The

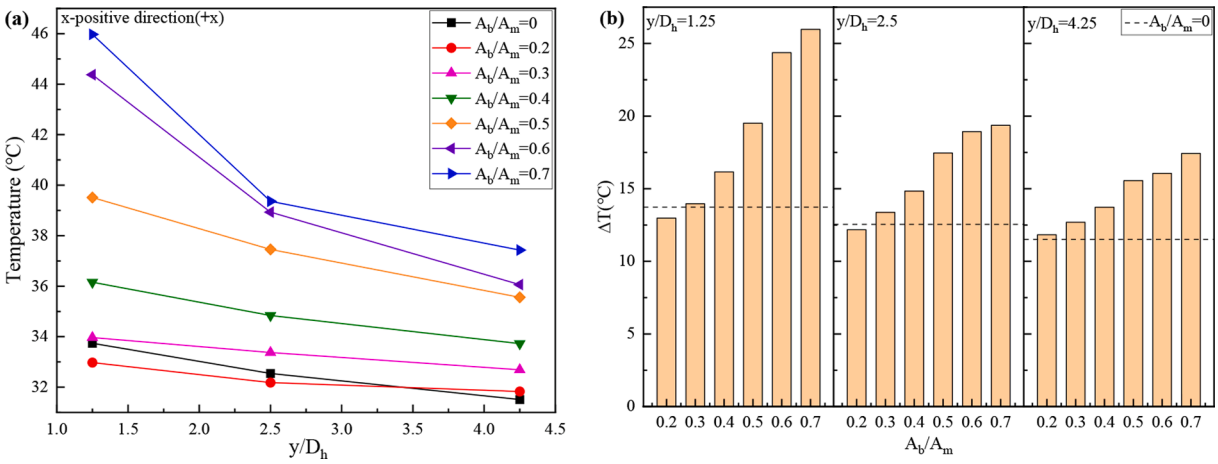

Fig. 8. Effect of baffle area ratios (R_A) in the +x direction on the axial average temperature and warming effect of thermal mixing.

flow distribution of the jet holes in the jet pipe tended to increase and then decay along the direction of the flow in the pipe. The maximum flow value occurs between x/L = 0.6 and 0.8 in the middle and rear sections of the jet pipe. This result is consistent with that of a previous study [23].

4.1. Effect of different baffle area ratios in the positive x-direction (+x) on flow and thermal mixing characteristics

Fig. 7 shows the temperature field distributions of the three measurement surfaces under the no-baffle condition. The jet pipe has a disturbing effect on the low-temperature main flow. The low-temperature mainstream flow through the jet pipe was faster on both sides and there was a local low-speed area behind the pipe wall. The high-temperature jet was ejected from two rows of jet holes in the jet pipe and was subjected to the disturbance and wrapping effect of the low-temperature mainstream, and intense convective heat transfer occurred behind the pipe wall. Therefore, as shown in Fig. 7, the low-temperature zone around the cross-section has the shape of a ring surrounding the high-temperature zone, and the low-temperature zone is larger in the area on the left and right sides. The high-temperature zone without baffles is concentrated in the middle of the measuring surface between $x/D_h = 0.5$ and 1.1, corresponding to the maximum jet pipe flow zone. The highest temperature in the high-temperature zone is only 54.8 °C in the $y/D_h = 1.25$ plane. From $y/D_h = 1.25$ to 4.25, the temperature distribution contours became increasingly sparse with increasing mixing displacement (i.e., mixing time), and the high- and low-temperature zones gradually decrease, indicating a deepening of the thermal mixing process.

Fig. 8 shows the effect of different baffle area ratios in the main flue on the average axial temperature after mixing and after inserting the baffle in the +x direction. As the baffle area ratio increased, the average axial temperature gradually increased after the thermal mixing. The highest average surface temperature of 45.97 °C was achieved at the 0.7 working condition. The warming effect reached a maximum value of 25.97 °C, an increase of up to 89.06 % relative to the no-baffle condition. The dashed line in Fig. 8(b) represents the temperature results for the no-baffle case (Case 1). A lower baffle area ratio had a very weak effect on the average temperature increase behind thermal mixing, and the average temperature increase on some of the measurement surfaces was even lower than that of the no-baffle case in the case for $R_A = 0.2$.

The distribution of the time-averaged temperature field after thermal mixing in the $y/D_h = 1.25$, $y/D_h = 2.5$, and $y/D_h = 4.25$ measurement surfaces with different baffle area ratios in the main flue after installation of the baffle in the +x direction is shown in Fig. 9. Compared with Fig. 7, the installation of the baffle increased the temperature on the left side of the measured section and reduced the extent of the low-temperature zone. The area of the local sub-high-temperature zone increased as the area ratio of the installed baffle increased, whereas that of while the surrounding low-temperature zone gradually decreased. The high-temperature zone is very pronounced for $R_A = 0.6$ and 0.7, with a maximum temperature of 67.8 °C in the high-temperature zone. However, within $y/D_h = 1.25$, the low-temperature zone was more pronounced on the right-hand side in the presence of a baffle than in the absence of a baffle. The presence of the baffle narrowed the flow cross section in the main flow tube, the local flow velocity increased and the flow rate of the low-temperature gas through the region increased per unit time; thus, the low-temperature zone was obvious. As the flow proceeded, the cross-sectional area recovered and the thermal mixing process increased. Within $y/D_h = 4.25$ plane, the right-hand low-temperature zone gradually decreased. In the $y/D_h = 1.25$ and 2.5 measurement planes, the temperature contours became denser as the ratio of baffle area in the main flue increased, indicating that the higher the temperature distribution gradient, the more uneven the thermal mixing.

The effects of the baffles on the local flow and thermal mixing characteristics were analyzed in conjunction with the simulation results. Fig. 10 shows a partial cross-section of the temperature distribution at the center of the jet hole, including the no-baffle condition with different baffle area ratios in the main flue (i.e., cases 2–7). In the region without baffles,the high-temperature zone behind the pipe wall tended to increase and then decrease in the center cross-section of jet holes, corresponding to the flow distribution characteristics along the jet hole.

The thermal mixing process between fluids is closely related to the state of the jet injected into the main flow [28]. After the jet was injected into the main flow at a certain initial velocity, the original flow direction was changed by the disturbance of the main flow, forming a new jet trajectory. The change in the jet trajectory significantly affected the macroscopic heat and mass transfer processes between the high and low-temperature fluid elements and the thermal mixing process. Several related studies have shown that the jet trajectory is mainly determined by the velocity ratio (R_u), density ratio (R_ρ) and compressibility of the flow [29]. Eq. (9) is typically used to correlate the jet trajectories.

$$R_u = \frac{U_J}{U_m} \tag{7}$$

$$R_\rho = \frac{\rho_J}{\rho_m} \tag{8}$$

$$\frac{y}{R_u} = A\left(\frac{x}{R_u d}\right)^B \rightarrow y = Ax^B(R_u d)^{1-B} \tag{9}$$

where U_J and U_m denote the jet and mainstream velocities, respectively, ρ_J and ρ_m represent the densities of the jet and main flow fluids,

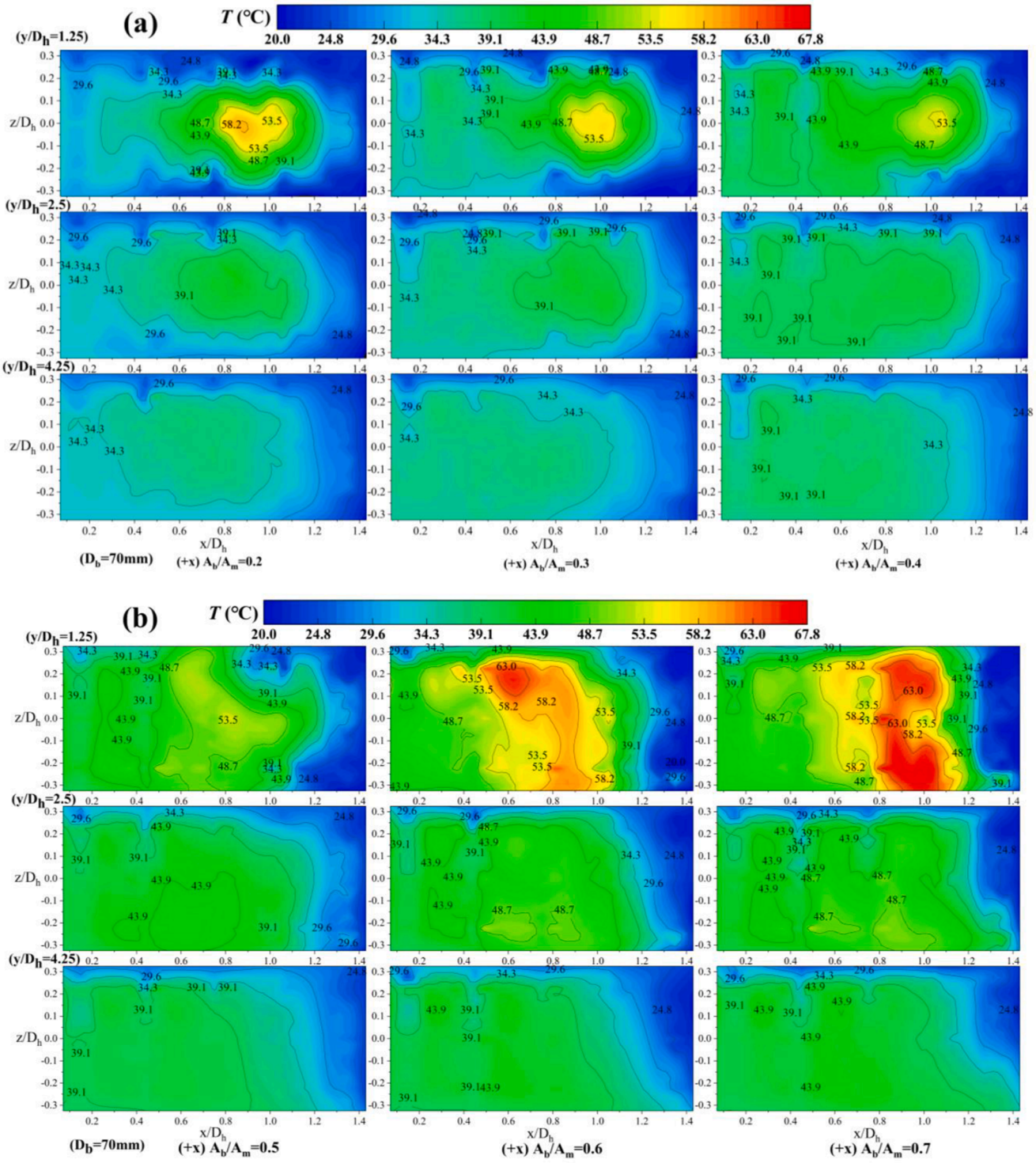

Fig. 9. Temperature distributions for cases 2–7. (a) Case 2–4, +x, R_A = 0.2, 0.3, 0.4; (b) Case 5–7, +x, R_A = 0.5, 0.6, 0.7.

respectively, and *d* is the diameter of the jet orifice or nozzle. Parameters A and B were factors determined by the experimental conditions, and ρ_j, ρ_m, and d remained constant during the experiment. The flow velocity ratio (R_u) determines the trajectory of the jet in the main flow.

As shown in Fig. 10, the presence of the baffle caused a significant change in the trajectory of the high-temperature jet behind the baffle when compared to the temperature distribution in the cross-section at the center of the jet hole at the same location. The blocking effect of the baffle caused a rapid drop in the flow velocity in the flow field behind. This area lacks the main flow, and the high-temperature jet retains its initial flow path, which is ejected from the jet holes in the pipe wall at a certain inclination angle. The jet orifice flow gradually increases along the direction of the jet flow. The amount of generated jet flow increases, and the high-temperature jet hits the tube wall and flows against it. Part of the fluid changes its direction and flows back towards the mainstream. When the flow rate of the high-temperature jet produced by the jet orifice increases to a certain level, the reverse flow of the high-temperature fluid forms a disturbance around the wall of the jet pipe, extending the residence time in this region.

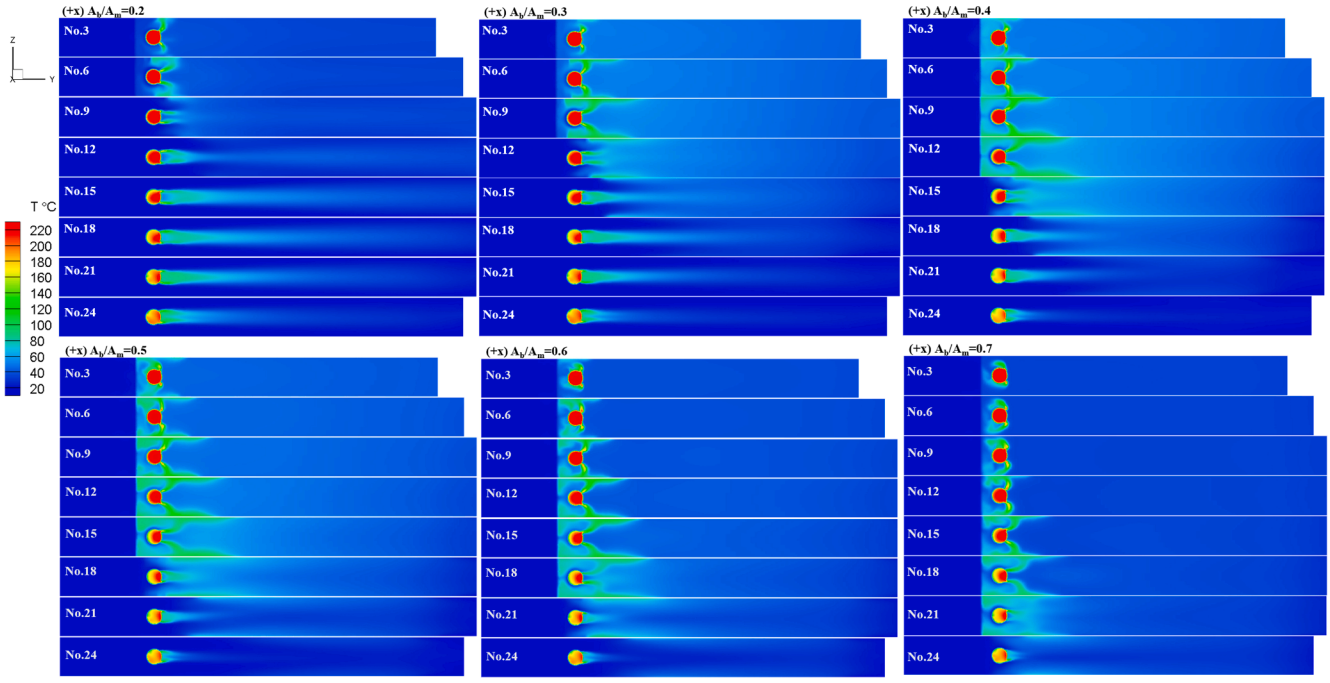

Fig. 10. Temperature contours of the transverse section in the center of partial jet holes. (Cases 2–7).

Meanwhile, the high-temperature jet retained its initial velocity along the direction of the jet pipe (+x-direction) and converged towards the low-temperature mainstream, which enhanced the thermal mixing effect at local positions to some extent. For the frontmost jet hole, the high-temperature jet flow generated is small and insufficient to hit the main flue wall, but still creates a high-temperature zone behind the flow. Because the main flue outlet has a necking structure, the main flow is faster on the unbaffled side. When the flow passes through the necking structure, it creates a backflow to the non-mainstream area on the baffled side. The generated return flow is close to the other side of the main flue wall. Therefore, the cold return flow is wrapped around the high-temperature jet from the front jet hole and flows in the opposite direction.

In Fig. 10, the presence of the baffle directly changes the flow trajectory of the rear high-temperature circular hole jet. Compare the temperature contours of the cross section at the center of jet holes at the same position in different cases, such as the high temperature zone formed by the 24th round hole jet. The high-temperature zone formed is continuously reduced with an increase in the baffle area. As the baffle area ratio increases, the flow cross section narrows, the local flow velocity of the cold flow gas increases and the wrapping effect on the high-temperature jet is enhanced. The flow of the LTFG for heat exchange with the HTFG increases per unit time, causing the high-temperature zone to shrink significantly. The baffle blocks part of the main flow, so that the jet ejected from the round hole behind it retains its original flow trajectory, and flows at an angle to both sides, as presented by the third and sixth round holes in case 2 in Fig. 10. At the same time, the circular hole jet has the velocity of the HTFG in the original pipe along the +x direction. The circular hole jet flow at the edge of the baffle exists in a transitional state. For example, the 9th hole of case 2 in Fig. 10(a), the R_A of case 2 is 0.2 and the baffle is 60 mm long, and its edge position is exactly the same height as the center section of the 9th hole in 3D space. Therefore, only a small part of the LTFG through this location, and the ability to wrap the HTFG at this location is limited. The trajectory of the high temperature jet is changed to a certain extent, but it is not completely converged, and there is separation in the middle of the formed high temperature region. Similar transition state exists in every case, such as the 12th round hole in case 3.

As the baffle increases, the blocking of the main flow covers a wider area. The circular hole jet with higher flow rate is no longer trapped by the low temperature main stream and ejects to both sides of the pipe wall. After hitting the inner wall of both sides of the flue, the direction and momentum of the jet change significantly, and it will flow along the wall. he partially rebounded high temperature jet converges between the jet tube and the baffle, forming a local reflow high temperature area, which enhances the thermal mixing effect to a certain extent.

The dimensionless parameter ζ_T is used to evaluate the degree of temperature distribution non-uniformity in the flue cross-section to visually compare the temperature distribution non-uniformity in the measurement plane after thermal mixing. The parameter is based on the overall calculation of the time-averaged temperature at all measurement points within the measurement plane. Its validity has been verified in studies by Lou [30] and Gou et al.[31] The formulas are shown in Eqs. (10)–(12):

$$\theta = \frac{T - T_0}{T_{max} - T_0} \tag{10}$$

$$\sigma_T = \sqrt{\frac{\left[\sum_{i=1}^{n} (\theta_i - \overline{\theta})^2\right]}{n}} \tag{11}$$

$$\zeta_T = \frac{\sigma_T}{\sqrt{\overline{\theta}(1 - \overline{\theta})}} \tag{12}$$

where T_{max} is the highest temperature within the $y/D_h = 1.25$ cross-section, T_0 is the main flow temperature, and T represents the time-averaged temperature at each measurement point. θ is a dimensionless parameter indicating the temperature in the measurement plane and $\overline{\theta}$ indicates the average value of the dimensionless temperature θ. Clearly, θ ranges from zero to one. σ_T is the dimensionless total standard deviation of the measured temperature. σ_T has a maximum value of $\sigma_T = \overline{\theta}(1 - \overline{\theta})$ indicating that the hot and cold gases are completely unmixed and are at a minimum value of $\sigma_T = 0$ at complete mixing. ζ_T takes values from 0 to 1. When $\zeta_T = 0$, the temperatures at each point in the section are exactly equal to achieve perfect mixing. When $\zeta_T = 1$, the hot and cold gases are completely unmixed, and the temperature

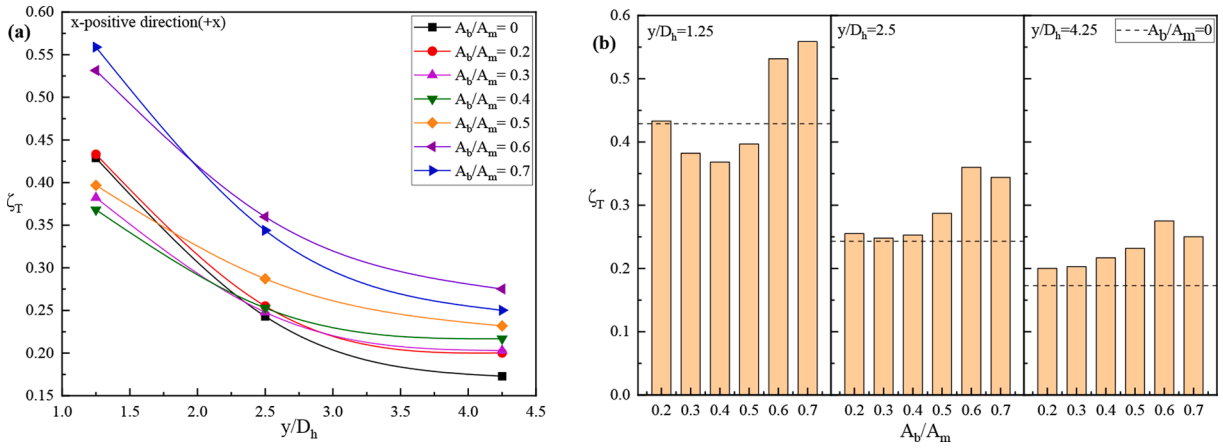

Fig. 11. Thermal mixing temperature inhomogeneity for different baffle area ratios in the +x direction (a) with y/D_h and (b) R_A.

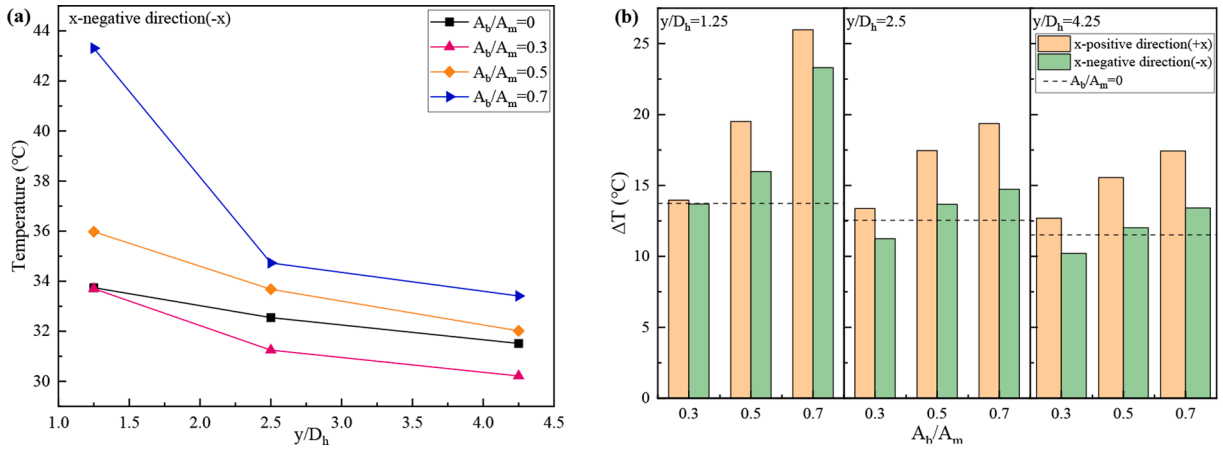

Fig. 12. Effect of baffle setting directions on the axial average temperature and warming effect of thermal mixing.

distribution is the most uneven.

Fig. 11 shows the thermal mixing inhomogeneity coefficients for different baffle area ratios in the main flue. The dashed line in Fig. 11(b) indicates the calculated temperature inhomogeneity coefficient without baffles. As the ratio of the baffle area increases, the temperature inhomogeneity after thermal mixing decreases and then increases in the y/D_h = 1.25 cross-section. The temperature inhomogeneity reaches a minimum value of $\zeta_T = 0.3682$ for the case of $R_A = 0.4$, which is 14.16 % lower than that of the no-baffle case. Meanwhile, the temperature distribution inhomogeneity coefficients forR_A = 0.6 and 0.7 are higher in the three measurement surfaces, indicating that the large ratio of the baffle area in the main flue leads to the extremely inhomogeneous temperature distribution. The temperature inhomogeneities for R_A = 0.3, 0.4, and 0.5 are lower than those for the no-baffle case at the y/D_h = 1.25 section but higher than that of the no-baffle case at the y/D_h = 4.25 section. This indicates that the upstream flow field created by the baffle is, to some extent, not conducive to promoting the thermal mixing of HLTFG during the flow mixing process. As the distribution of the flow along the jet hole tends to increase and then decreases slightly, the jet flow generated by the jet hole in the right-hand region within the measurement plane accounts for most of the HTFG, as shown in Fig. 6. The installation of the baffle into the flue from the +x direction concentrates the low-temperature mainstream gas on the right side of the flue cross-section, enhancing the thermal mixing process between the LTFG and HTFG. Therefore, when the baffle area is 0.3–0.5 in the main flue, the temperature inhomogeneity coefficient within the y/D_h = 1.25 cross-section is reduced relative to the case without baffles. The baffle area ratio of 0.2 has a relatively small effect on the main flow deflection, so the temperature inhomogeneity coefficient at the 1.25 section is very close to that of the case without baffles.

4.2. *Effect of different baffle installation directions on flow and thermal mixing characteristics*

Fig. 12 shows the effect of different baffle area ratios in the main flue on the average axial temperature after thermal mixing when baffles are inserted in reverse (−x) direction from the x-axis. Fig. 12(b) shows a comparison of the warming effect of inserting baffles in the +x direction. The experimental results showed that the average surface temperature increased as the baffle area ratio increases, with the same variation law for the three measurement surfaces. However, Fig. 12(b) shows the warming effect of inserting the baffle in the −x direction is lower than that of inserting the baffle in the +x direction and is most obvious for theR_A = 0.5 and 0.7 cases.

Comparing Fig. 7 and Fig. 13, it can be seen that after installing the baffle in the −x direction, the right side of the low-temperature zone in the section shrinks, and the high-temperature zone increases significantly. Simultaneously, the temperature on the left side of the low-temperature zone increases. As the area of the baffle increases, the overall low-temperature zone on the measurement surface decreases, and the local high-temperature zone increases significantly, resulting in a denser temperature distribution contour. On the right side of the temperature distribution cloud, two local high-temperature zones are symmetrically distributed along the central axis. Because the baffle

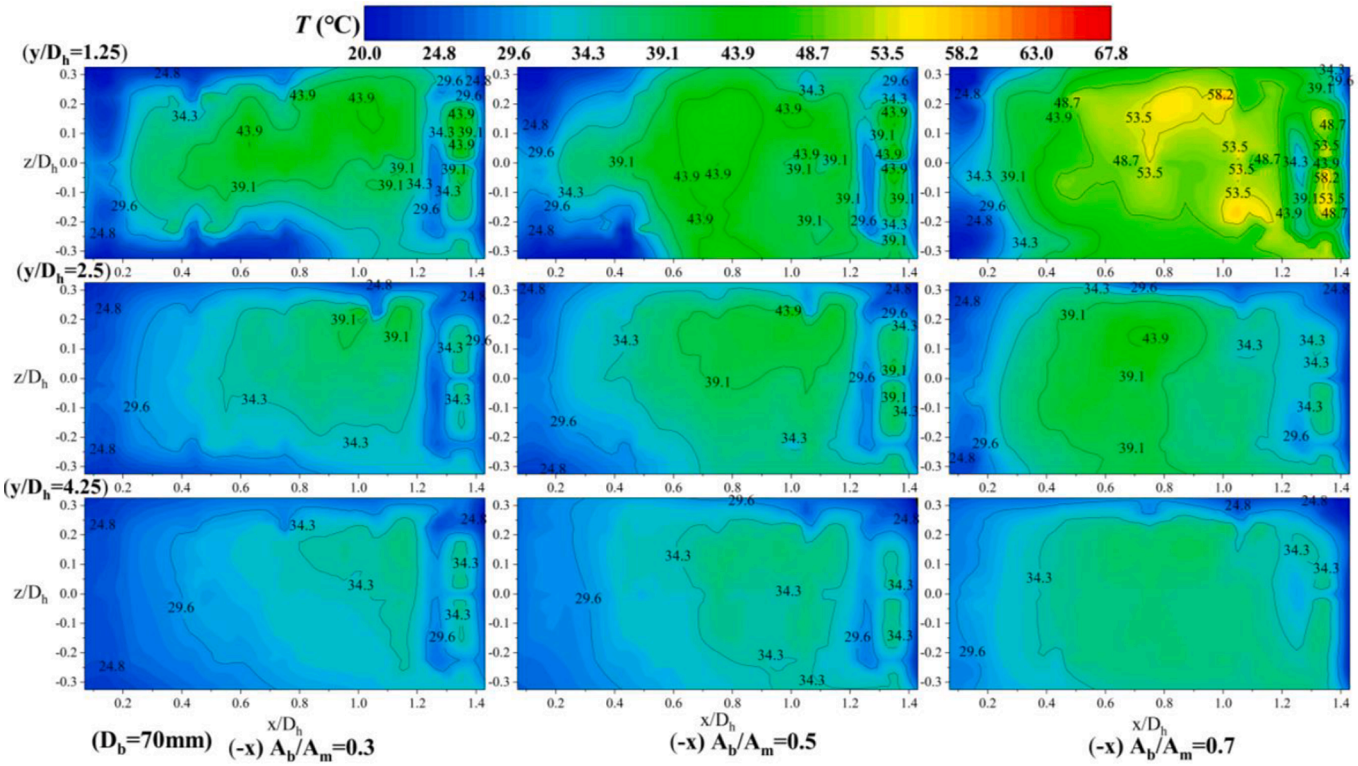

Fig. 13. Temperature distribution for cases 8–10 (−x) at y/Dh = 1.25, y/Dh = 2.5 and y/Dh = 4.25.

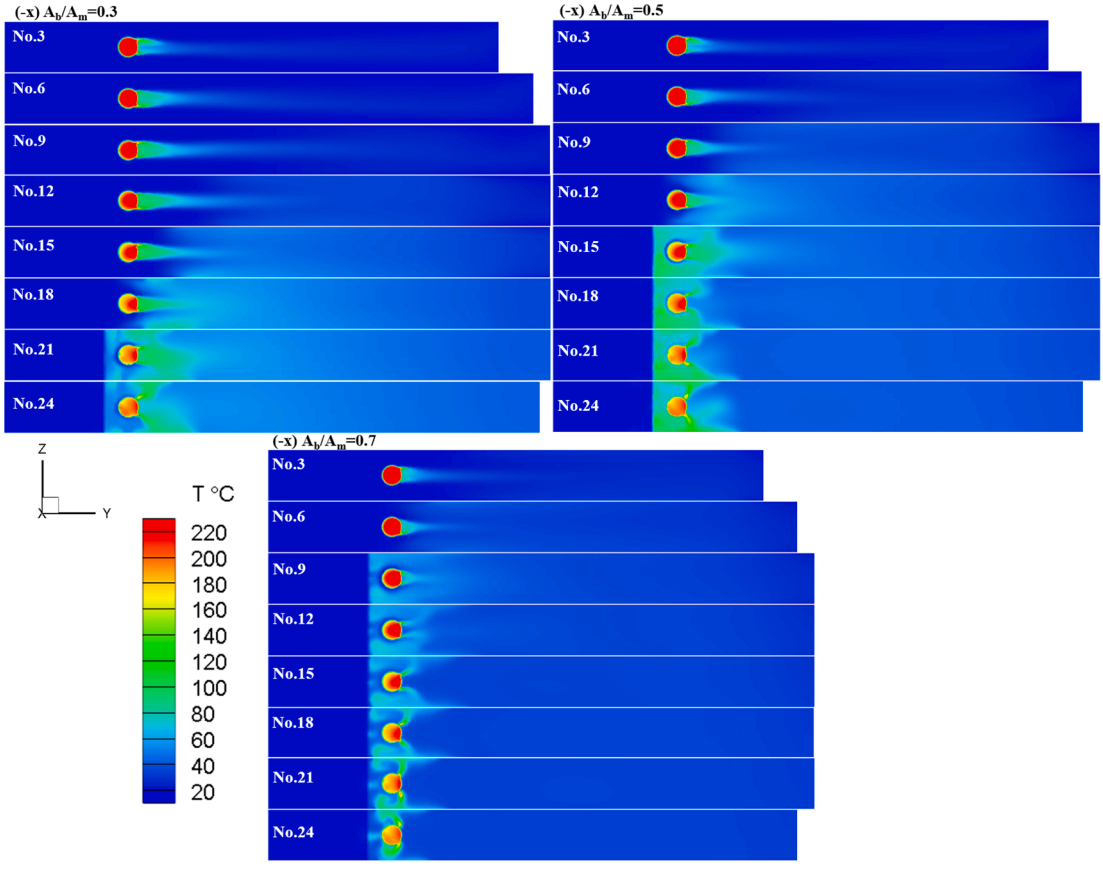

Fig. 14. Temperature contours of the transverse section in the center of partial jet holes. Case 8–10 (−x, R_A = 0.3, 0.5, 0.7).

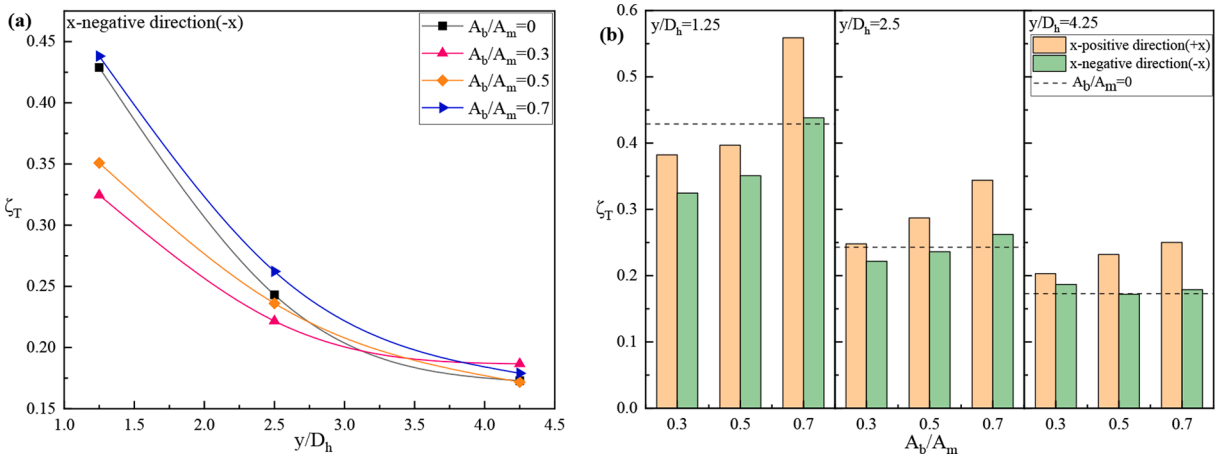

Fig. 15. Thermal mixing temperature inhomogeneity for different baffle setting directions (a) with y/Dh and (b) R_A.

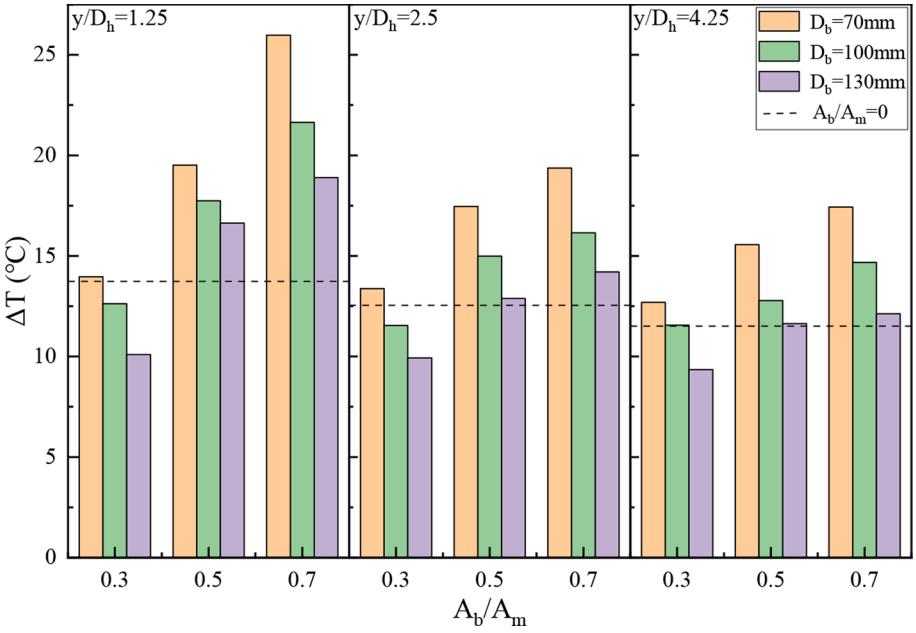

Fig. 16. Effect of different baffle positions on the average warming effect of each section after thermal mixing.

inserted in the −x direction blocks the main flow in this area, the bottom of the jet pipe and the jet hole at the end of the pipe wall retain the initial flow trajectory, and after hitting the inner wall of the main flue, a high-temperature return zone is formed. The backflow phenomenon of the described jet trajectory is shown in Fig. 14 and is the most evident forR_A = 0.7. Owing to the lack of high-speed cold-flow gas wrapped in the area behind the baffle, the high-temperature gas flow is relatively large, and the flow velocity from the jet hole is faster. After hitting the main flue wall, the effect of the jet reflection is enhanced, and the hot gas flow remains and gathers toward the back of the flow and flows toward the area where the baffle is not set. The overall jet velocity is low, the flow ratio to the main flow is reduced, and the temperature inhomogeneity coefficient after thermal mixing is reduced. As shown in Fig. 15, the installation of the baffle from the −x direction increases the baffle area ratio from 0.3 to 0.7, and the temperature inhomogeneity after thermal mixing gradually decreases. Compared with inserting the baffle from the −x axis in the positive direction, the temperature inhomogeneity coefficients decrease for the same baffle area ratios.

4.3. Effect of baffle position to jet pipe center distance (D_b) on flow and thermal mixing characteristics

Fig. 16 shows the effect of different baffle positions on the axially oriented face-averaged warming effect after thermal mixing, with the baffle inserted in the +x direction. As the baffle position moves away from the center of the jet pipe, that is, Db increases from 70 to 130 mm, the surface-averaged warming effect after thermal mixing decreases. The same trend was observed exists for different baffle area ratios. At lower baffle area ratios e.g., R_A=0.3, the baffle at D_b = 100 and 130 mm had a lower heating effect than the unbaffled condition at the y/D_h = 1.25 and 2.5 cross sections. As shown in Fig. 17, as the distance between the baffle and the center of the jet pipe increased, the high-temperature zone within the measurement surface gradually decreased, and the surrounding low-temperature zone expanded significantly for the same percentage of baffle area. The temperature distribution contours became sparse and the temperature gradient decreased. According to the calculation results shown in Fig. 18, the temperature-distribution inhomogeneity coefficient gradually decreased. When the main flow flows through the baffle position, the flow cross section in the tube suddenly decreases owing to the presence of the baffle. After passing through the

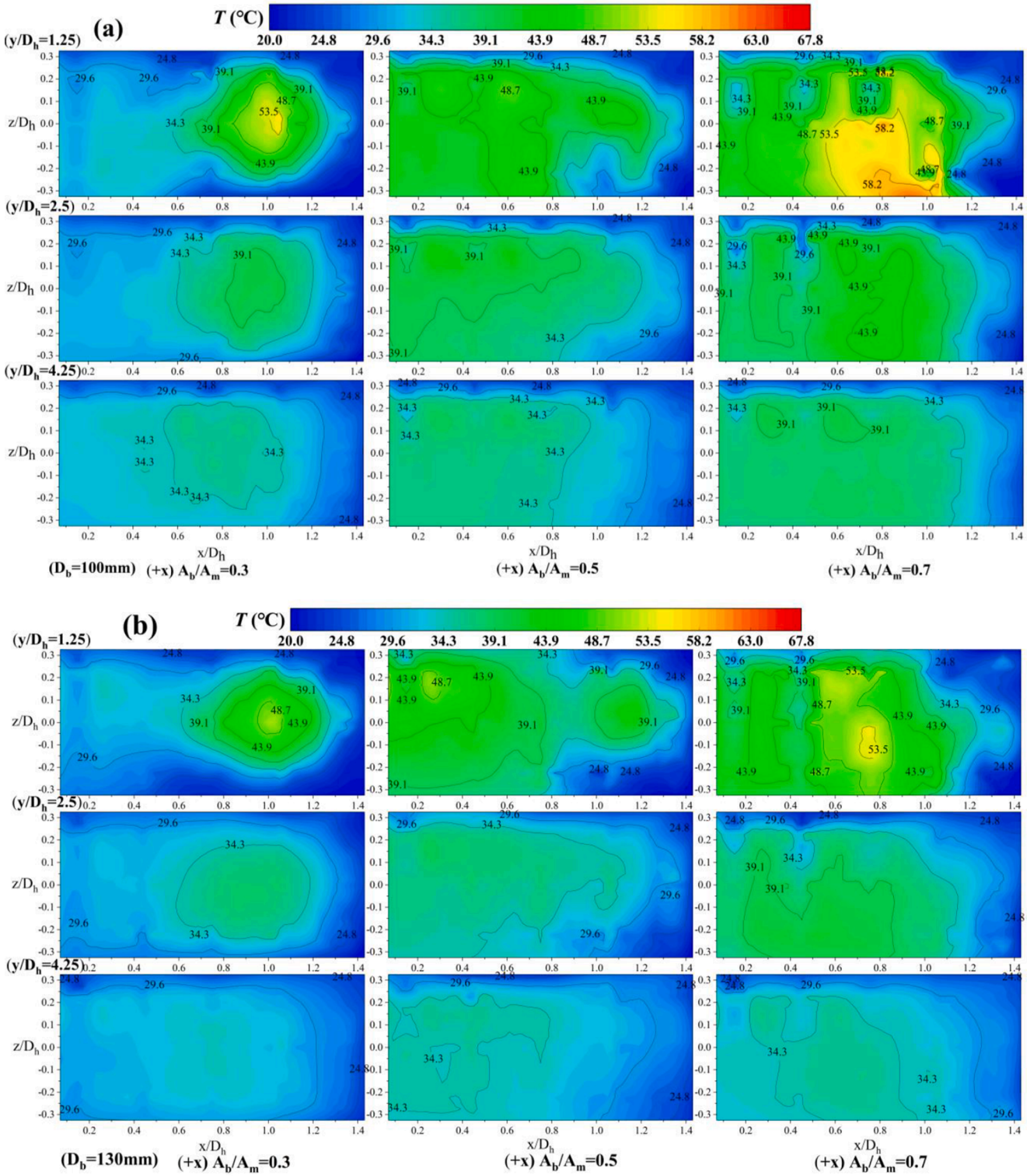

Fig. 17. Temperature distributions for cases 11–16 at y/Dh = 1.25, y/Dh = 2.5 and y/Dh = 4.25. (a) Cases 11–13, D_b = 100 mm; (b) Cases 14–16, D_b = 130 mm.

baffle, the flow cross-section in the tube is quickly restored, and the main flow tends to shift towards the non-main flow area behind the baffle while retaining the original local flow. Consequently, most of the main flow passes through the zone of relatively concentrated flow in the jet pipe. A small part then passes through the jet orifice where the original jet flow is small, promoting hot mixing. In this case, the thermal mixing effect is improved, the surface heating effect is reduced, and the temperature inhomogeneity coefficient of the measuring surface becomes lower.

Compared to the studies in the previous sections, the effect of D_b on flow and thermal mixing is by intervening in the mainstream fluid earlier in the direction of incoming flow. Baffle installation mode and baffle opening both interfere with the flow by directly changing the flow section state. Early intervention of the flow enhances the disturbance effect of the fluid itself and develops more rapidly in the process of hot mixing with high temperature gas. The hot mixing process is accelerated

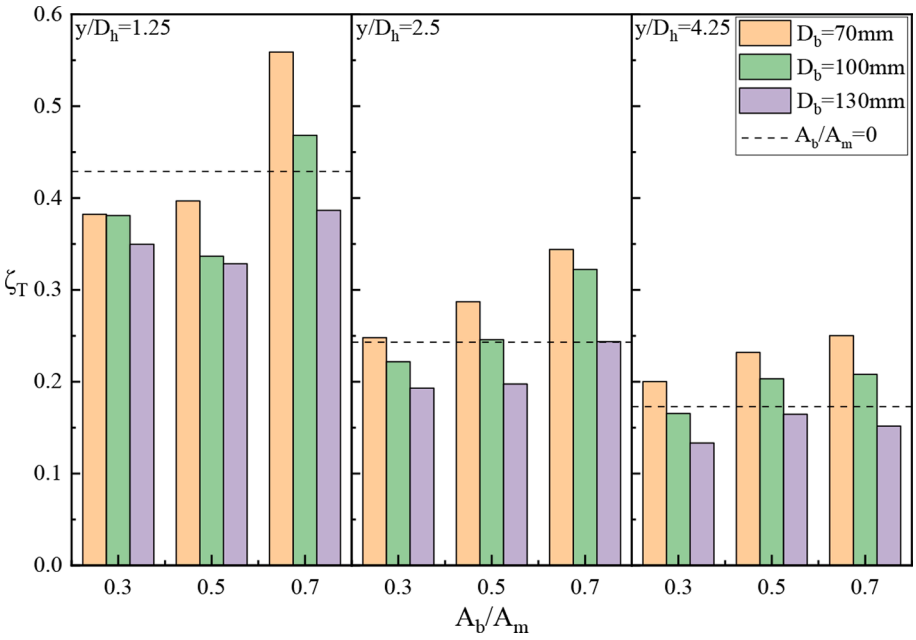

Fig. 18. Effect of different baffle positions on the temperature inhomogeneity coefficient of thermal mixing.

and the temperature mixing inhomogeneity is decreased obviously.

5. Conclusion

Based on the built experimental system, this study investigated the flow and thermal mixing characteristics of a multijet bypass flue with a main flue baffle during low load operation. The results were analyzed in conjunction with CFD numerical simulations. Several interesting research conclusions were drawn as follows:

(1) The average axial surface temperature after thermal mixing increased with increasing baffle area ratio (R_A) in the main flue. The increase in the average temperature was more evident at higher area ratios. The same trend was observed for different baffle setting directions (+x and −x directions) and baffle positions.

(2) With the same baffle position, the temperature inhomogeneity (ζ_T) after thermal mixing decreased and then increased in the y/Dh = 1.25 cross-section as the baffle area ratio increased. ζ_T reached its minimum value in the case of R_A = 0.4. At the same time, higher baffle area ratios led to a nonuniform temperature distribution after thermal mixing, with ζ_T being higher on all three measurement surfaces for R_A = 0.6 and 0.7.

(3) The baffles were set in different directions to create different thermal mixing effects. The average temperature of the thermally mixed surface after the installing of the baffle in the −x direction was lower than that in the +x direction, and the warming effect was not as effective as that in the +x direction. However, the temperature inhomogeneity coefficient after thermal mixing with the same baffle area ratio was lower than that of the +x direction installation. The temperature distribution was more uniform, and the thermal mixing characteristics were better.

(4) The presence of a baffle significantly altered the flow trajectory of the high-temperature jet ejected from the rear jet pipe in the low-temperature main stream region. The jet retains its flow state when ejected from the jet hole, and after striking the wall of the main flue, it creates a localized backflow, extending the residence time. A high-temperature zone was formed on the front side of the jet pipe, which affected the thermal mixing characteristics.

(5) With the same baffle area ratio in the main flue, as the distance from the baffle to the center of the jet pipe increased from 70 mm to 130 mm, the average axial surface temperature after thermal mixing decreased and the warming effect weakened, while the temperature inhomogeneity (ζ_T) gradually decreased. This phenomenon indicates that the earlier occurrence of the baffle-blocking effect over this distance results in better thermal mixing in the downstream flow field; however, the warming effect is reduced.

CRediT authorship contribution statement

Yize Zhang: Conceptualization, Methodology, Investigation, Data curation, Writing – original draft, Writing – review & editing. **Ao Zhang:** Investigation. **Lei Zhang:** Investigation. **Kelang Jin:** Investigation. **Hao Zhou:** Conceptualization, Methodology, Resources, Supervision, Project administration, Funding acquisition.

Declaration of Competing Interest

The authors declare that they have no known competing financial interests or personal relationships that could have appeared to influence the work reported in this paper.

Data availability

Data will be made available on request.

Acknowledgement

Supported by the Fundamental Research Funds for the Central Universities (2022ZFJH04).

References

[1] M. Richter, G. Oeljeklaus, K. Görner, Improving the load flexibility of coal-fired power plants by the integration of a thermal energy storage, Appl. Energy 236 (2019) 607–621.

[2] M. Qing, S. Lei, F. Kong, L. Liu, W. Zhang, L. Wang, T. Guo, S. Su, S. Hu, Y. Wang, J. Xiang, Analysis of ammonium bisulfate/sulfate generation and deposition characteristics as the by-product of SCR in coal-fired flue gas, Fuel 313 (2022), 122790.

[3] Y. Ni, Y. Rong, X. Yu, S. Huang, X. Xue, H. Zhou, Experimental study on the effects of reheat temperatures on the ammonium bisulfate and ash blend deposition, Fuel 324 (2022), 124719.
[4] M. Qing, X. Zhang, S. Lei, L. Liu, G. Zhang, S. Wang, B. Zhao, W. Zhang, L. Wang, S. Su, S. Hu, Y. Wang, J. Xiang, Insights into the deposition and transformation characteristics of ammonium bisulfate on the fly ash as the by-product of SCR in air preheater, Fuel 324 (2022), 124582.
[5] Y. Han, G. Xu, Q. Zheng, C. Xu, Y. Hu, Y. Yang, J. Lei, New heat integration system with bypass flue based on the rational utilization of low-grade extraction steam in a coal-fired power plant, Appl. Therm. Eng. 113 (2017) 460–471.
[6] H. Zhou, J. Chen, M. Zhou, K. Cen, Experimental investigation on the mixing performance of heating gas into the low temperature sintering flue gas selective catalyst reaction facilities, Appl. Therm. Eng. 115 (2017) 378–392.
[7] W. Zhou, K. Xing, S. Dou, Q. Yang, X. Xu, Distribution characteristics of a supercritical hydrocarbon fuel jet injected into a high-speed crossflow, Fuel 333 (2023), 126497.
[8] T. Yi, B.R. Halls, N. Jiang, J. Felver, M. Sirignano, B.L. Emerson, T.C. Lieuwen, J. R. Gord, S. Roy, Autoignition-controlled flame initiation and flame stabilization in a reacting jet in crossflow, Proc. Combust. Inst. 37 (2019) 2109–2116.
[9] R. Moradi, M. Mosavat, M.B. Gerdroodbary, A. Abdollahi, Y. Amini, The influence of coolant jet direction on heat reduction on the nose cone with Aerodome at supersonic flow, Acta Astronaut. 151 (2018) 487–493.
[10] H. Zhou, X. Guo, M. Zhou, W. Ma, M.W. Dahri, K. Cen, Optimization of ammonia injection grid in hybrid selective non-catalyst reduction and selective catalyst reduction system to achieve ultra-low NOx emissions, J. Energy Inst. 91 (2018) 984–996.
[11] M. Zhou, R. Kulenovic, E. Laurien, Experimental investigation on the thermal mixing characteristics at a 90° T-Junction with varied temperature differences, Appl. Therm. Eng. 128 (2018) 1359–1371.
[12] Y. Amini, M. Mokhtari, M. Haghshenasfard, M.B. Gerdroodbary, Heat transfer of swirling impinging jets ejected from Nozzles with twisted tapes utilizing CFD technique, Case Stud. Therm. Eng. 6 (2015) 104–115.
[13] A. Edalatpour, A. Hassanvand, M.B. Gerdroodbary, R. Moradi, Y. Amini, Injection of multi hydrogen jets within cavity flameholder at supersonic flow, Int. J. Hydrogen Energy 44 (2019) 13923–13931.
[14] R. Moradi, A. Mahyari, M.B. Gerdroodbary, A. Abdollahi, Y. Amini, Shape effect of cavity flameholder on mixing zone of hydrogen jet at supersonic flow, Int. J. Hydrogen Energy 43 (2018) 16364–16372.
[15] C. Tao, H. Zhou, Correlation analysis of oxy-fuel jet in cross-flow on thermoacoustic instability in a model gas turbine combustor, Aerosp. Sci. Technol. 106 (2020), 106184.
[16] M. Zhou, R. Kulenovic, E. Laurien, T-junction experiments to investigate thermal-mixing pipe flow with combined measurement techniques, Appl. Therm. Eng. 150 (2019) 237–249.
[17] C.H. Lin, M.S. Chen, Y.M. Ferng, Investigating thermal mixing and reverse flow characteristics in a T-junction by way of experiments, Appl. Therm. Eng. 99 (2016) 1171–1182.
[18] C.H. Lin, Y.M. Ferng, Investigating thermal mixing and reverse flow characteristics in a T-junction using CFD methodology, Appl. Therm. Eng. 102 (2016) 733–741.
[19] Z. Tan, P. Jin, Y. Zhang, G. Xie, Flow and thermal performance of a multi-jet twisted square microchannel heat sink using CuO-water nanofluid, Appl. Therm. Eng. 225 (2023), 120133.
[20] B. Wu, G. Tang, X. Chen, C.Q. Zhou, C.P. Colella, T. Okosun, Optimization of an urea decomposition chamber using CFD and VR, Appl. Therm. Eng. 70 (2014) 827–837.
[21] M.P. Boruah, P.R. Randive, S. Pati, Hydrothermal performance and entropy generation analysis for mixed convective flows over a backward facing step channel with baffle, Int. J. Heat Mass Transf. 125 (2018) 525–542.
[22] J. Chen, N. Li, Y. Ding, J.J. Klemeš, P.S. Varbanov, Q. Wang, M. Zeng, Experimental thermal-hydraulic performances of heat exchangers with different baffle patterns, Energy 205 (2020), 118066.
[23] Y. Zhang, M. Zhang, H. Zhou, Mixing performance of preheated flue gas entering selective catalytic reactor under low loads, Appl. Therm. Eng. 224 (2023), 120049.
[24] S. Hu, Y. Ni, Y. Zhang, W. Ma, H. Li, K. Cen, H. Zhou, Visualization research on ash deposition characteristics of Zhundong coal in a vertical liquid slagging cyclone furnace, Fuel Process. Technol. 238 (2022), 107506.
[25] H. Zhu, G. Xie, R. Zhu, B. Sunden, Comparisons on flow characteristics and film cooling performance of cylindrical and sister holes with/without internal coolant crossflow, Int. J. Therm. Sci. 182 (2022), 107791.
[26] T. Sriveerakul, S. Aphornratana, K. Chunnanond, Performance prediction of steam ejector using computational fluid dynamics: Part 1. Validation of the CFD results, Int. J. Therm. Sci. 46 (2007) 812–822.
[27] J. Dong, Q. Hu, M. Yu, Z. Han, W. Cui, D. Liang, H. Ma, X. Pan, Numerical investigation on the influence of mixing chamber length on steam ejector performance, Appl. Therm. Eng. 174 (2020), 115204.
[28] A. Hewes, L. Mydlarski, Multi-scalar mixing in turbulent coaxial jets, J. Fluid Mech. 961 (2023).
[29] Z. Chen, K. Hu, Y. Mao, X. Su, X. Yuan, Simple integral model for trajectories of jet deflection in crossflow, Phys. Fluids 33 (2021), 111703.
[30] P. Luo, H. Jia, C. Xin, G. Xiang, Z. Jiao, H. Wu, An experimental study of liquid mixing in a multi-orifice-impinging transverse jet mixer using PLIF, Chem. Eng. J. 228 (2013) 554–564.
[31] X. Guo, H. Zhou, H. Shi, Y. Li, K. Zhang, M. Zhou, Promotion of the mixing performance of heated gas and low-temperature sintering gas in selective catalytic reaction facilities, Exp. Therm. Fluid Sci. 94 (2018) 258–280.